Available online at www.sciencedirect.com
ScienceDirect
Journal of Sound and Vibration 307 (2007) 834–848
JOURNAL OF SOUND AND VIBRATION
www.elsevier.com/locate/jsvi

Effect of cable flexibility on transient response of a beam–pendulum system

Michael El-Raheb

1000 Oakforest Lane, Pasadena, CA 91107, USA

Received 12 March 2007; received in revised form 23 June 2007; accepted 18 July 2007
Available online 29 August 2007

Abstract

The effect on beam–pendulum response of cable flexibility is studied. The system is forced at its base by a prescribed damped periodic oscillation. Response from cable tension is estimated at a delayed time step from known variables computed at a previous time step in a linear modal analysis. The effects of base excitation and force from cable flexibility are included adopting the static–dynamic superposition method. Two distinct non-dimensional parameters κ_o and μ_r, control the linear modal response of beam and pendulum. Unlike periodic excitation where the pendulum may be used as an absorber of energy, in transient response the conditions leading to absorption do not apply. Even for large pendulum swings, cable flexibility has a negligible effect on flexural response considering that cable tension dominated by high frequencies is larger than the shear force Q_{xxL} it transmits at the beam-free end. Contrary to its effect on flexure, cable flexibility induces a high-frequency axial force comparable to Q_{xxL}.

1. Introduction

The model of a flexible beam coupled to a pendulum is often considered as an approximation to large flexible structures with an appendage. Crespo et al. [1] studied the effect of approximations on the dynamic response of a cantilever with tip mass. Cuvalci [2] and Ertas and Cuvalci [3] studied the nonlinear absorber with varying orientation. Yaman et al. [4] studied a cantilever beam with tip-mass and pendulum adopting finite elements. For sinusoidal excitation, energy transfer between beam and pendulum is largest at the auto-parametric condition, implying that the pendulum may act as a vibration absorber. Yaman and Sen [5] and Yaman and Sen [6] treated the same problem simplifying the beam–pendulum to a 2-degree-of-freedom oscillator to investigate the effect of pendulum orientation on its effectiveness as a vibration absorber. Cicek and Ertas [7] studied experimentally the coupled system under random excitation. Dumas et al. [8] studied experimentally the performance of a 3-stage low-frequency vibration isolation chain made of vertical Euler-spring and a self-damped pendulum. Mikhlin and Reshetnikova [9] studied the nonlinear 2-degree-of-freedom system of a massive linear oscillator and a light nonlinear oscillator acting as an absorber to the former adopting nonlinear normal modes. Oguamanan et al. [10] and Oguamanan and Hansen [11] studied the dynamic response of an overhead crane system. Ju et al. [12] studied linear dynamic response of tower cranes

E-mail address: mertrident@earthlink.net

0022-460X/$ - see front matter
doi:10.1016/j.jsv.2007.07.025

coupled with the pendulum motions of the payload adopting finite elements for the tower crane and rigid-body kinetics for the pendulum. Their analysis concludes that the lowest tower and pendulum modes dominate response, and that nonlinearity is week for planar pendulum motions. Yang et al. [13] studied the dynamics of a slewing flexible beam attached to a pendulum.

All references above treat linear and nonlinear periodic motions. The present study considers transient response of a vertical cantilever beam–pendulum system from prescribed base motion adopting a modal decomposition. Prescribed motion at the base is included utilizing the static–dynamic superposition method [14,15]. Modal response relies on two non-dimensional parameters: a beam wave number $\kappa_o = l_b(m_b\omega_o^2/(E_bI_b))^{1/4}$ and a mass ratio $\mu_r = m_bl_b/m_p$, where E_bI_b is flexural stiffness, l_b is length, m_b is mass per unit length, and m_p, ω_o are pendulum mass and frequency. Curves of system resonances versus κ_o with μ_r as parameter reveal the strong influence the first 2 modes have on response. The lowest of this dyad is a beam dominant mode with frequency below ω_o, while the second is a pendulum dominant mode with frequency above ω_o. Unlike periodic excitation where the pendulum may be used as an absorber of energy, in transient response the conditions leading to absorption do not apply.

For long slender beams, the effect of cable flexibility and inertia is evaluated adopting a time-delayed method. Since the driving force of these motions along the cable is the nonlinear centrifugal force, response of the cable is computed at some time step t based on the centrifugal force determined from a previous time step $t-\Delta t$. This time-delayed cable tension then acts as an external concentrated body force at the beam-free end, appearing as an inhomogeneity in the beam equation of motion. The effect on beam extensional response of cable flexibility is then evaluated by solving the coupled beam–cable extensional equations from a time-delayed centrifugal excitation.

2. Coupled beam–pendulum

The 1-D Euler equations and boundary conditions of a cantilever beam with a pendulum pivoted at its free end are (see Fig. 1(a) and Appendix A):

$$E_bI_b\partial_{xxxx}w + m_b\ddot{w} = p_o(x,t); \quad -l_b/2 \leqslant x \leqslant l_b/2, \tag{1a}$$

$$w_0 = 0, \quad w_0' = 0, \quad w_0 \equiv w(-l_b/2), \tag{1b}$$

$$w_L'' = 0, \quad E_bI_bw_L''' = m_pl_p\ddot{\varphi}, \quad w_L \equiv w(l_b/2), \tag{1c}$$

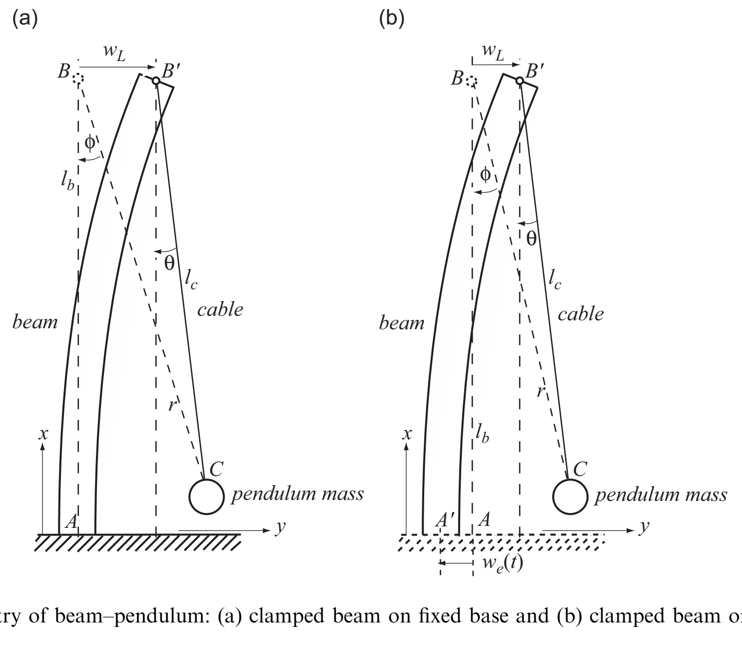

Fig. 1. Geometry of beam–pendulum: (a) clamped beam on fixed base and (b) clamped beam on moving base.

$$\ddot{\varphi} + \omega_o^2 \varphi = \omega_o^2 w_L / l_c, \quad \omega_o = \sqrt{g/l_c}, \tag{1d}$$

where $(\cdot)$ is derivative w.r.t. time t, x the axial coordinate, $(\ )'$ is derivative w.r.t. x, l_b the beam length, E_b, I_b are Young's modulus and cross-sectional moment of inertia, m_b the mass per unit length, w the lateral displacement, φ the angle between undeformed beam axis B–A and radial vector r along (B–C) from the undeformed free end B to the displaced pendulum mass C (Fig. 1(a)), g the acceleration of gravity, l_c the length of the inextensional massless cable, m_p the pendulum mass, and $p_o(x, t)$ the applied lateral distributed load per unit length. Boundary conditions (1b) apply to clamping at the fixed base, while boundary conditions (1c) apply to the free end connected to a pendulum whose motion is governed by Eq. (1d). For harmonic motions in time with radian frequency ω, the homogeneous Eqs. (1a) and (1d) admit a solution

$$w = \mathrm{e}^{\hat{\mathrm{i}}\omega t} \sum_{n=1}^{4} A_n \mathrm{e}^{k_n x}, \quad k_{1,2} = \pm \hat{\mathrm{i}}\hat{k}, \quad k_{3,4} = \pm \hat{k}, \quad \hat{\mathrm{i}} = \sqrt{-1}, \tag{2a}$$

$$\hat{k} l_b = \kappa = l_b \left(m_b \omega^2 / (E_b I_b) \right)^{1/4} = \hat{k}_o l_b \tilde{\omega}^{1/2}, \tag{2b}$$

$$\begin{aligned} \hat{k}_o l_b &= l_b \left(m_b \omega_o^2 / (E_b I_b) \right)^{1/4}, \quad \tilde{\omega} = \omega / \omega_o \\ \varphi &= \mathrm{e}^{\hat{\mathrm{i}}\omega t} w_L / \left(l_c (1 - \tilde{\omega}^2) \right). \end{aligned} \tag{2c}$$

This reduces the second boundary condition in Eq. (1c) to

$$(1 - \tilde{\omega}^2)(m_b l_b / m_p)/(\hat{k}_o l_b \tilde{\omega}^{1/2}) w_L''' / \hat{k}^3 + w_L = 0. \tag{3}$$

It is clear from Eqs. (2) and (3) that there are 3 distinct non-dimensional parameters controlling free dynamic motion

$$\kappa_o = \hat{k}_o l_b = l_b \left(m_b \omega_o^2 / (E_b I_b) \right)^{1/4} \Rightarrow \hat{k} l_b = \kappa = \kappa_o \tilde{\omega}^{1/2}, \tag{4a}$$

$$\mu_r = m_b l_b / m_p, \tag{4b}$$

$$\tilde{\omega} = \omega / \omega_o \tag{4c}$$

for wave number, mass, and frequency, respectively. Substituting Eq. (2) in Eqs. (1b) and (1c) yields the eigenproblem

$$\begin{gathered} \mathbf{M}\mathbf{A} = \mathbf{0}, \quad \mathbf{A} = \{A_1, A_2, A_3, A_4\}^{\mathrm{T}} \Rightarrow \det|\mathbf{M}| = 0, \\ \mathbf{M} = \begin{bmatrix} \mathrm{e}^{-\alpha_1} & \mathrm{e}^{-\alpha_2} & \mathrm{e}^{-\alpha_3} & \mathrm{e}^{-\alpha_4} \\ \tilde{k}_1 \mathrm{e}^{-\alpha_1} & \tilde{k}_2 \mathrm{e}^{-\alpha_2} & \tilde{k}_3 \mathrm{e}^{-\alpha_3} & \tilde{k}_4 \mathrm{e}^{-\alpha_4} \\ \tilde{k}_1^2 \mathrm{e}^{\alpha_1} & \tilde{k}_2^2 \mathrm{e}^{\alpha_2} & \tilde{k}_3^2 \mathrm{e}^{\alpha_3} & \tilde{k}_4^2 \mathrm{e}^{\alpha_4} \\ (\beta \tilde{k}_1^3 + 1)\mathrm{e}^{\alpha_1} & (\beta \tilde{k}_2^3 + 1)\mathrm{e}^{\alpha_2} & (\beta \tilde{k}_3^3 + 1)\mathrm{e}^{\alpha_3} & (\beta \tilde{k}_4^3 + 1)\mathrm{e}^{\alpha_4} \end{bmatrix}, \\ \alpha_n = k_n l_b / 2, \quad \tilde{k}_n = k_n / \hat{k}, \quad \beta = (1 - \tilde{\omega}^2)\mu_r / (\kappa_o \tilde{\omega}^{1/2}). \end{gathered} \tag{5}$$

Eq. (5) determines the eigenset $\{\omega_j, \psi_j(x)\}$. Forced response from $p_o(x, t)$ proceeds adopting the modal expansion

$$w(x, t) = \sum_j a_j(t) \psi_j(x). \tag{6}$$

where $a_j(t)$ are generalized coordinates. Substituting Eq. (6) in Eq. (1a) and enforcing orthogonality of ψ_j yields

$$\begin{aligned}
&\ddot{a}_j(t) + \omega_j^2 a_j(t) = \tilde{N}_{fj}(t), \quad \tilde{N}_{fj} = N_{fj}(t)/N_{jj},\\
&N_{fj}(t) = \int_{-l_b/2}^{l_b/2} p_o(x,t)\psi_j(x)\,\mathrm{d}x,\\
&N_{jj} = m_b \int_{-l_b/2}^{l_b/2} \psi_j^2(x)\,\mathrm{d}x + m_p\left(\psi_j(l_b/2)/(1-\tilde{\omega}_j^2)\right)^2.
\end{aligned} \tag{7}$$

A $p_o(x, t)$ in the form

$$p_o(x,t) = (H(x-x_1) - H(x-x_2))f(t) \tag{8}$$

simplifies N_{fj} in Eq. (7) to $N_{fj}(t) = f(t)N_{pj}$ where $N_{pj} = \int_{x_1}^{x_2} \psi_j(x)\,\mathrm{d}x$ and $H(x)$ is the Heaviside function. Eq. (7) then admits the solution

$$a_j(t) = A_{pj}\sin(\omega_j t) + B_{pj}\cos(\omega_j t) + \left(N_{pj}/(N_{jj}\omega_j)\right)\int_0^t f(\tau)\sin\left(\omega_j(t-\tau)\right)\mathrm{d}\tau. \tag{9}$$

Constants A_{pj}, B_{pj} are determined from the initial conditions $w(x,0), \dot{w}(x,0)$.

If the base moves laterally with prescribed displacement $w_e(t)$ (see Fig. 1(b)) with $p_o(x, t) = 0$, the method of static–dynamic superposition is employed. $w(x, t)$ is expressed as the sum of a dynamic solution $w_d(x, t)$ satisfying homogeneous boundary conditions and a static solution $w_s(x)$ satisfying inhomogeneous boundary conditions:

$$w(x,t) = w_d(x,t) + w_s(x)f(t), \tag{10}$$

where $f(t)$ is time dependence of the displacement prescribed at the base. Consequently, $w_d(x, t)$ satisfies the same boundary conditions as in Eqs. (1b) and (1c) at both ends:

$$w_{d0} = 0, \quad w'_{d0} = 0, \quad w_{d0} \equiv w_d(-l_b/2), \tag{11a}$$

$$w''_{dL} = 0, \quad E_b I_b w'''_{dL} = m_p l_p \ddot{\varphi}, \quad w_{dL} \equiv w_d(l_b/2). \tag{11b}$$

$w_s(x)$ satisfies the static equation

$$\partial_{xxxx} w_s = 0 \tag{12}$$

with boundary conditions

$$w_{s0} = 1, \quad w'_{s0} = 0, \quad w_{s0} \equiv w_s(-l_b/2), \tag{13a}$$

$$w''_{sL} = 0, \quad w'''_{sL} = 0, \quad w_{sL} \equiv w_s(l_b/2). \tag{13b}$$

Solving Eq. (12) with boundary conditions Eq. (13) yields

$$w_s(x) = 1. \tag{14}$$

Eq. (14) specifies a rigid body translation.

Expanding $w_d(x, t)$ in its eigenfunctions $\psi_j(x)$ following the same steps that lead to Eq. (5):

$$w_d(x,t) = \sum_j a_j(t)\psi_j(x), \quad \psi_j(x) = \sum_{n=1}^{4} A_{nj}\mathrm{e}^{k_{nj}x}, \quad -l_b/2 \leqslant x \leqslant l_b/2. \tag{15}$$

In Eq. (15), k_{nj} is defined in Eq. (2a) for the jth eigenfunction. Substituting Eq. (9) in the homogeneous form of Eq. (1a) and enforcing orthogonality of $\psi_j(x)$ produces

$$\begin{aligned}
&\ddot{a}_j(t) + \omega_j^2 a_j(t) = -\tilde{N}_{bj}\ddot{f}(t),\\
&\tilde{N}_{bj} = (N_{bj}/N_{jj}), \quad N_{bj} = m_b\int_{-l_b/2}^{l_b/2} w_s(x)\psi_j(x)\,\mathrm{d}x \equiv m_b\int_{-l_b/2}^{l_b/2}\psi_j(x)\,\mathrm{d}x.
\end{aligned} \tag{16}$$

N_{jj} is defined in Eq. (7). The solution to Eq. (16) takes the form

$$a_j(t) = A_j \sin(\omega_j t) + B_j \cos(\omega_j t) - (\tilde{N}_{bj}/\omega_j) \int_0^t \ddot{f}(\tau) \sin\big(\omega_j(t-\tau)\big)\, \mathrm{d}\tau. \tag{17}$$

Constants A_j, B_j are determined from the initial conditions

$$w(x,0) = 0, \quad \dot{w}(x,0) = 0. \tag{18}$$

Substituting Eq. (9) in Eq. (18) yields

$$A_j = -(\tilde{N}_{bj}/\omega_j)\dot{f}(0), \quad B_j = -\tilde{N}_{bj} f(0). \tag{19}$$

For a base undergoing damped periodic motions of the form

$$f(t) = a_b \mathrm{e}^{-\zeta_b t} \sin(\omega_b t)[H(t) - H(t - t_s)], \tag{20a}$$

$$\dot{f}(t) = a_b \mathrm{e}^{-\zeta_b t}(\omega_b \cos(\omega_b t) - \zeta_b \sin(\omega_b t)), \tag{20b}$$

$$\ddot{f}(t) = a_b \mathrm{e}^{-\zeta_b t}\Big[\Big(\omega_j^2 - \zeta_b^2\Big) \sin(\omega_b t) + 2\zeta_b\omega_j \cos(\omega_b t)\Big], \tag{20c}$$

then $f(0) = 0$ and $\dot{f}(0) = a_b\omega_b$.

3. Cable flexibility

For a long elastic cable and large m_p, the effect on transmitted force at the pivot from extensional motions of the cable is considered. These motions are driven by the nonlinear centrifugal force from pendulum sway (see Appendix A, Eq. (A.4a)). Coupling of cable flexibility to beam flexure is presented first, followed by coupling to beam extension.

3.1. Coupling to beam flexure

To include this effect in the linear flexural treatment of Section 1, a time-delayed approximation is adopted in the integration of the generalized coordinates Eq. (16). Consider an elastic cable fixed at the pivot end and attached to the mass m_p at its other end. The cable extentional equation of motion and boundary conditions are

$$\begin{aligned} &E_c A_c \partial_{rr} u_c + \rho_c A_c \partial_{tt} u_c = 0, \quad 0 \leqslant r \leqslant l_c, \\ &u_c(0,t) = 0, \quad E_c A_c \partial_r u_c(l_c, t) + m_p \partial_{tt} u_c(l_c, t) = F_c(t) \equiv m_p l_c \dot{\varphi}^2, \end{aligned} \tag{21}$$

where r is the coordinate along the cable, E_c, ρ_c, A_c are cable modulus, density and cross-sectional area, u_c is elastic displacement, and F_c is centrifugal force. To solve Eq. (21), apply the static–dynamic superposition procedure utilized in Section 1. Express $u_c(r, t)$ as the sum of a dynamic solution $u_{cd}(r, t)$ and a static solution $u_{cs}(r)$

$$\begin{aligned} &u_c(r,t) = u_{cd}(r,t) + u_{cs}(r) F_c(t), \\ &u_{cd}(0,t) = 0, \quad E_c A_c \partial_r u_{cd}(l_c, t) + m_p \partial_{tt} u_{cd}(l_c, t) = 0, \\ &u_{cs}(0) = 0, \quad E_c A_c \partial_r u_{cs}(l_c) = 1. \end{aligned} \tag{22}$$

For harmonic motions in time with frequency ω, the solution to u_{cd} and dispersion relation satisfying Eq. (22) are:

$$\begin{aligned} &u_{cd}(r,t) = \sin(k_c r)\mathrm{e}^{\hat{\imath}\omega t}, \quad k_c = \omega/c_c, \quad c_c = \sqrt{E_c/\rho_c}, \\ &(E_c A_c / m_p l_c)\cos(k_c l_c) - \omega^2 \sin(k_c l_c) = 0. \end{aligned} \tag{23}$$

The solution to u_{cs} is

$$u_{cs}(r) = r/(E_c A_c). \tag{24}$$

Expanding u_{cd} in its eigenfunctions

$$u_{cd}(r,t) = \sum_j a_{cj}(t)\psi_{cj}(r), \quad \psi_{cj}(r) = \sin(k_{cj}r), \tag{25}$$

then substituting Eqs. (22)–(25) in Eq. (21) yields

$$\begin{gathered}\ddot{a}_{cj}(t) + \omega_{cj}^2 a(t) = -\tilde{N}_{cbj}\ddot{F}_c(t), \quad \tilde{N}_{cbj} = (N_{cbj}/N_{cjj}), \\ N_{cbj} = \rho_c A_c \int_0^{l_c} u_{cs}(r)\psi_{cj}(r)\,\mathrm{d}r, \quad N_{cjj} = \rho_c A_c \int_0^{l_c} \psi_{cj}^2(r)\,\mathrm{d}r + m_p\psi_{cj}^2(l_c).\end{gathered} \tag{26}$$

The solution to Eq. (26) takes the form

$$a_{cj}(t) = A_{cj}\,\sin(\omega_{cj}t) + B_{cj}\,\cos(\omega_{cj}t) - (\tilde{N}_{cbj}/\omega_{cj})\int_0^t \ddot{F}_c(\tau)\sin\big(\omega_{cj}(t-\tau)\big)\,\mathrm{d}\tau. \tag{27}$$

Constants A_{cj}, B_{cj} are determined from the initial conditions

$$u_c(r,0) = 0, \quad \dot{u}_c(r,0) = 0. \tag{28}$$

Substituting Eq. (22) in Eq. (28), with use made of Eq. (24) and Eq. (25) yields

$$A_{cj} = -(\tilde{N}_{cbj}/\omega_{cj})\dot{F}_c(0), \quad B_{cj} = -\tilde{N}_{cbj}F_c(0). \tag{29}$$

The incremental dynamic tension in the cable follows:

$$\Delta T_c(r,t) = E_c A_c \sum_j a_{cj}(t)\psi'_{cj}(r) + F_c(t). \tag{30a}$$

In turn, the incremental shear force at the pivot is

$$\Delta Q_{xxc}(t) = \Delta T_c(0,t)\varphi(t). \tag{30b}$$

Since ΔQ_{xxc} is a nonlinear function of φ, it can be included in the linear analysis assuming that ΔQ_{xxc} is a known external body force from an earlier time step $t-\Delta t$ during the numerical integration. This means that in Eq. (1a) the body force $p_o(x, t)$ at time step t is related to ΔQ_{xxc} by

$$p_o(x,t) = \delta(x - l_b/2)\Delta Q_{xxc}(t - \Delta t). \tag{31}$$

$\delta(x)$ is Dirac's delta function. This adds a term to the particular integral of Eq. (17) similar to the one in Eq. (9) as follows:

$$\begin{aligned} a_j(t) = {} & A_j\,\sin(\omega_j t) + B_j\,\cos(\omega_j t) - (\tilde{N}_{bj}/\omega_j)\int_0^t \ddot{f}(\tau)\sin\big(\omega_j(t-\tau)\big)\,\mathrm{d}\tau \\ & + \Big(\psi_j(l_b/2)/(N_{jj}\omega_j)\Big)\int_0^{t-\Delta t} \Delta Q_{xxc}(\tau)\sin\big(\omega_j(t-\tau)\big)\,\mathrm{d}\tau. \end{aligned} \tag{32}$$

3.2. Coupling to beam extension

The coupled extensional equations of beam and cable are:

$$E_b A_b \partial_{xx} u_b - \rho_b A_b \partial_{tt} u_b = 0, \quad 0 \leqslant x \leqslant l_b, \tag{33a}$$

$$E_c A_c \partial_{rr} u_c - \rho_c A_c \partial_{tt} u_c = 0, \quad 0 \leqslant r \leqslant l_c, \tag{33b}$$

$$u_b(0,t) = 0, \tag{33c}$$

$$u_b(l_b,t) = u_c(0,t), \tag{33d}$$

$$E_b A_b \partial_x u_b(l_b,t) = E_c A_c \partial_r u_c(0,t), \tag{33e}$$

$$E_c A_c \partial_r u_c(l_c,t) + m_p \partial_{tt} u_c(l_c,t) = F_c(t). \tag{33f}$$

Eqs. (33a) and (33b) are the extensional equations for beam and cable, respectively, where x is a coordinate along the beam with origin at the fixed end, r is coordinate along the cable with origin at the pivot $x = l_b$, ρ_b, A_b are beam density and cross-sectional area, and u_b, u_c are axial displacements of beam and cable. Eq. (33c) is beam fixed end condition, Eqs. (33d) and (33e) are continuity of displacement and axial force at the beam–cable junction, and Eq. (33f) is dynamic equilibrium of pendulum mass and cable tension forced by $F_c(t)$ the centrifugal force along r from pendulum swing.

For harmonic motions in time with radian frequency ω, the solutions to Eqs. (33a) and (33b)) satisfying Eqs. (33c)–(33e) are:

$$\begin{aligned} u_b(x,t) &= c_1 \sin(k_{eb}x)\mathrm{e}^{\hat{\mathrm{i}}\omega t}, \quad k_{eb} = \omega/c_{eb}, \quad c_{eb} = \sqrt{E_b/\rho_b}, \\ u_c(r,t) &= (c_3 \sin(k_{ec}r) + c_4 \cos(k_{ec}r))\mathrm{e}^{\hat{\mathrm{i}}\omega t}, \quad k_{ec} = \omega/c_{ec}, \quad c_{ec} = \sqrt{E_c/\rho_c}, \\ c_3 &= c_1 \sin(k_{eb}l_b), \quad c_4 = c_1\beta_c \cos(k_{eb}l_b), \quad \beta_e = E_bA_bc_{ec}/(E_cA_cc_{eb}). \end{aligned} \tag{34}$$

Substituting Eq. (34) in Eq. (33f) yields the dispersion relation

$$\alpha_e(\beta_e cs_b cs_c - sn_b sn_c) - (\beta_e cs_b sn_c + sn_b cs_c) = 0, \quad \alpha_e = E_cA_ck_{ec}/(m_p\omega^2), \tag{35}$$

where cs, sn stand for cos and sin while subscripts b and c stand for $(k_{eb}l_b)$ and $(k_{ec}l_c)$. Eq. (35) determines the eigenset $\{\psi_{eb}(x), \psi_{ec}(r); \omega_{ec}\}_j$.

Since $F_c(t)$ is an inhomogeneity in boundary condition Eq. (33f), express u_b and u_c as

$$\begin{aligned} u_b(x,t) &= \sum_j a_{ej}(t)\psi_{ebj}(x) + u_{bs}(x)F_c(t), \\ u_c(r,t) &= \sum_j a_{ej}(t)\psi_{ecj}(r) + u_{cs}(r)F_c(t), \\ u_{bs}(x) &= x/E_bA_b, \quad u_{cs}(r) = l_b/E_bA_b + r/E_cA_c. \end{aligned} \tag{36}$$

u_{bs} and u_{cs} are static solutions satisfying the inhomogeneous boundary condition Eq. (33d) with $F_c = 1$. Substituting Eq. (36) in Eqs. (33a) and (33b) and enforcing orthogonality of the eigenfunctions determines equations in $a_{ej}(t)$ with solution

$$\begin{aligned} a_{ej}(t) &= A_{ej} \sin(\omega_{ecj}t) + B_{ej} \cos(\omega_{ecj}t) - \left(N_{ebj}/(N_{ejj}\omega_{ecj})\right) \int_0^t \ddot{F}_c(\tau)\sin\left(\omega_{ecj}(t-\tau)\right) \mathrm{d}\tau, \\ N_{ebj} &= \rho_bA_b \int_0^{l_b} u_{bs}(x)\psi_{ebj}(x)\,\mathrm{d}x + \rho_cA_c \int_0^{l_c} u_{cs}(r)\psi_{ecj}(r)\,\mathrm{d}r, \\ N_{ejj} &= \rho_bA_b \int_0^{l_b} \psi^2_{ebj}(x)\,\mathrm{d}x + \rho_cA_c \int_0^{l_c} \psi^2_{ecj}(r)\,\mathrm{d}r + m_p\psi^2_{ecj}(0), \\ A_{ej} &= -(N_{ebj}/N_{ejj})\dot{F}_c(0)/\omega_{ecj}, \quad B_{ej} = -(N_{ebj}/N_{ejj})F_c(0). \end{aligned} \tag{37}$$

4. Results

Fig. 2 plots the first 3 modes of the clamped beam for $\mu_r = 50$ and $\kappa_o = 1.98$. Note that only the first two resonances include motions of the pendulum. The first mode describes a pendulum dominant motion w_p that is in phase with the beam w. The second mode describes a w-dominant motion that is out-of-phase with w_p. This mode dyad exists independent of μ_r and κ_o. Starting with the third mode, the pendulum mass is almost motionless and the beam motion is the same as that of the lone beam. Consequently, the effect on response of the pendulum is primarily from the first mode dyad.

Fig. 3 plots the non-dimensional modal variables with wave number parameter κ_o for the first 3 modes and for 2 values of μ_r: 50 and 5. For small κ_o, $\tilde{\omega}_1 \approx 1$ while $\tilde{\omega}_2$ drops smoothly till $\kappa_o \approx 2$ near the coalescence of these 2 lines (Fig. 3(a1)). At that stage, the $\tilde{\omega}_1$ line changes path following that of the $\tilde{\omega}_2$ line and continues dropping smoothly with κ_o, while the $\tilde{\omega}_2$ line changes its path to that of the $\tilde{\omega}_1$ line close to $\tilde{\omega}_2 \approx 1$.

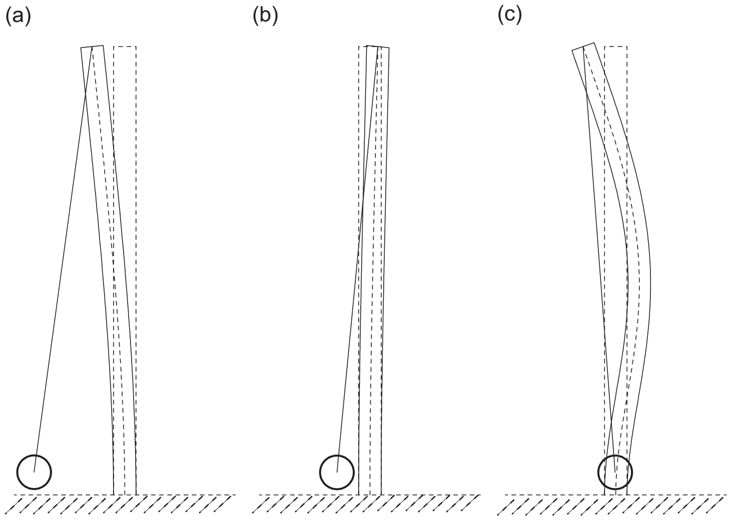

Fig. 2. Mode shapes: $\mu_r = 50$, $\kappa_o = 1.98$; (a) mode 1 $\omega_1/\omega_0 = 0.81$, (b) mode 2 $\omega_2/\omega_0 = 1.11$, and (c) mode 3 $\omega_3/\omega_0 = 5.61$.

This change in path and the nature of the mode are repeated when the $\tilde{\omega}_3$ and $\tilde{\omega}_2$ lines approach their coalescence at $\kappa_o \approx 4.5$. The reason for this change in path near coalescence stands on the uniqueness of the linear eigenstates insuring that different eigenfunctions cannot have the same frequency. Near coalescence of $\tilde{\omega}_1$ and $\tilde{\omega}_2$, the frequency separation between these 2 resonances is smallest and this condition may affect forced response by enabling energy transfer between the 2 modes.

Fig. 3(b1) plots κ/π for the first 3 modes. For small κ_o, the κ_1 line rises almost linearly then changes path near coalescence with the κ_2 line then follows a constant value of 0.6, the first cantilever mode of the lone beam. At this point, the κ_2 line continues along the κ_1 line before coalescence, till it approaches coalescence with the κ_3 line, and then follows a constant value of 1.5, the second cantilever mode of the lone beam.

Fig. 3(c1) plots w_L/w_{mx}. Note the smooth transition of the second mode line from $+1$ to -1 prior to the second coalescence point. Fig. 3(d1) plots $\log_{10}(\varphi l_p/w_{mx})$. Note that the first and second lines intersect near the first coalescence, while the second and third lines intersect near the second coalescence. Near these points, pendulum amplitude of the first dyad achieves a minimum.

Fig. 3(a2–d2) plots the non-dimensional variables for $\mu_r = 5$. Comparing corresponding lines for the two μ_r's reveals a similar behavior except that for $\mu_r = 5$, separation between the lines near coalescence is wider, and $\log_{10}(\varphi l_c/w_{mx})$ near the first coalescence is smaller (see Fig. 3(a2) and (d2)).

Since modal variables are unique near $\kappa_o \approx 2$, properties leading to that value are considered in the example to follow:

$$E_b I_b = 57.4\,\mathrm{N\,m^2}, \quad l_b = l_c = 5\,\mathrm{m}, \quad m_b = 0.7\,\mathrm{kg/m}, \quad m_p = 0.07\,\mathrm{kg}.$$

These properties are hypothetical and have been chosen so as to produce $\kappa_o = 1.98$. Parameters of the base excitation are $a_b = 1\,\mathrm{cm}$, $\Omega_b = 0.4\,\mathrm{Hz}$, and $\zeta_b = 0.3\,\mathrm{s^{-1}}$.

Fig. 4 plots beam and pendulum response for a base excitation with $a_b = 1\,\mathrm{cm}$ shown in Fig. 4(a). Fig. 4(b) plots w_L response of the beam at the free end. Magnitude of w_L is 4 times larger than a_b. At the start of motion, w_L is out-of-phase with base motion because $\omega_b > \omega_1$. After 7 s, w_L response attenuates temporarily because of energy transfer from beam to pendulum. During this time, pendulum motion φl_c in Fig. 4(c) reaches a maximum. For $t > 10\,\mathrm{s}$, pendulum motion resumes in phase with beam motion raising beam amplitude. During that short time interval $6 < t < 10\,\mathrm{s}$, velocity is reduced also (Fig. 4(d)). It follows that if the pendulum were arrested during this time interval, the beam might continue its free motion with smaller amplitude.

Fig. 5(a and b) plots response of the beam without pendulum. The w_L peak is the same as that with pendulum (Fig. 4(b)) but does not attenuate near $t = 7\,\mathrm{s}$. This implies that during this short time interval, attenuation of w_L in Fig. 4(a) is not caused by the time form of base excitation but by the temporary transfer of energy between beam and pendulum.

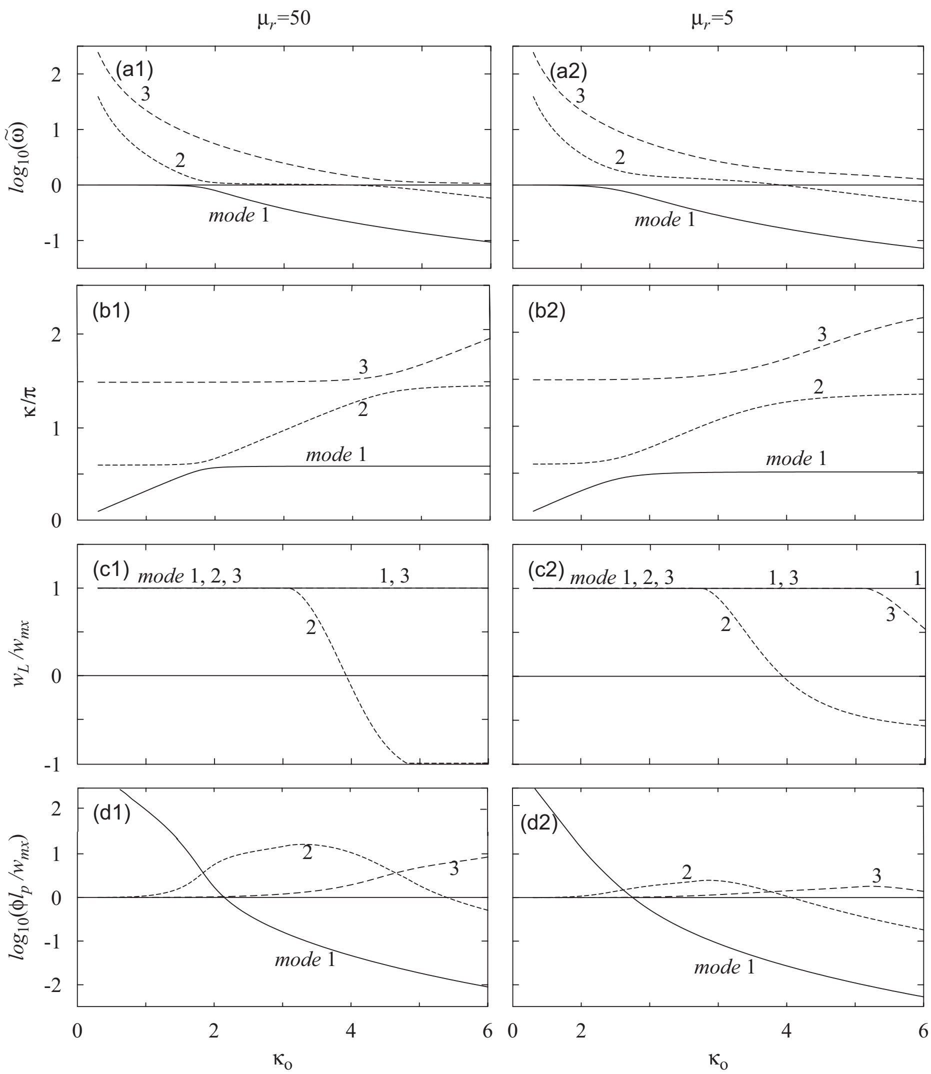

Fig. 3. Variation of non-dimensional variables with κ_o: (a1)–(d1) $\mu_r = 50$, (a2)–(d2) $\mu_r = 5$. ———, mode 1; - - - - -, mode 2; — — — —, mode 3.

The different stages of response appear in time-snapshots of the beam and pendulum shown in Fig. 6. At the start of motion, ($t = 0.5$ s) the beam is out-of-phase with base motion because $\omega_b > \omega_1$. Starting $5 < t < 11$ s, pendulum amplitude increases while that of the beam is reduced indicating a temporary transfer of energy. For $12 < t < 15$ s, beam amplitude reverts to its original value while pendulum amplitude is reduced.

For an elastic cable, assume $E_cA_c = 44.5N$ and $\rho_c = 1.1\,\mathrm{g/cm^3}$. Prior to coupling cable extensional motion to the beam, its effect is evaluated based on a prescribed oscillation $\varphi(t) = \sin(\omega_o t)$ producing the centrifugal force (see Eq. (A.6a))

$$F_c(t) = m_p l_c \dot{\varphi}^2 = m_p l_c (1 + \cos(2\omega_o t))/2, \quad \ddot{F}_c(t) = -2m_p l_c \omega_o^4 \cos(2\omega_o t). \tag{38}$$

Substituting Eq. (33) in Eqs. (27)–(30) determines cable response. In the analysis to follow, 25 terms are included in the modal expansion of Eq. (25).

In Fig. 7(a), peaks of cable extensional displacement $u_c(l_c, t)$ follow those of F_c (Eq. (33)) with period π/ω_o. Acceleration response (Fig. 7(b)) is modulated by cable extensional modes ω_{cj}, $j \geqslant 1$ noting that $\omega_{c1} \gg \omega_o$. Incremental cable tension ΔT_c (Fig. 7(c)) resembles acceleration (Fig. 7(b)) indicating that ΔT_c is dominated

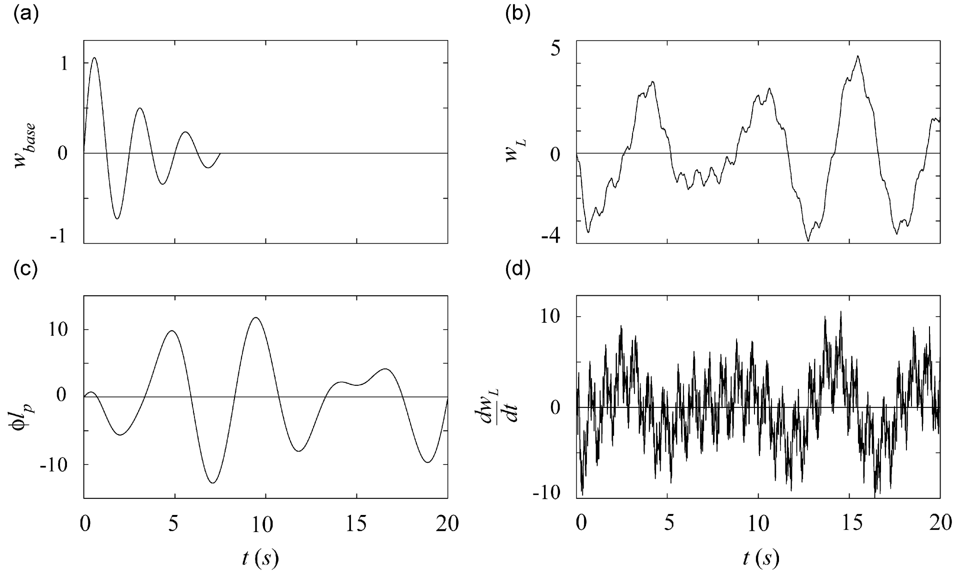

Fig. 4. Beam histories with pendulum: $a_b = 1$ cm, $\phi_{mx} = 0.025$ rad. (a) w_{base} (cm), (b) w_L (cm), (c) ϕl_{p} (cm), and (d) $\mathrm{d}w_L/\mathrm{d}t$ (cm/s).

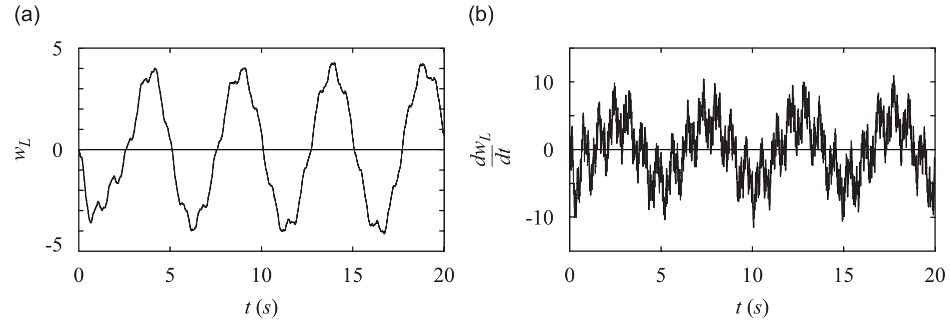

Fig. 5. Lone beam response: $a_b = 1$ cm; (a) w_L (cm) and (b) $\mathrm{d}w_L/\mathrm{d}t$ (cm/s).

by cable elastic response and not centrifugal force $F_c \approx 0.7$ N. ΔT_c (Fig. 7(c)) rises by more than an order of magnitude when cable flexibility is included. This is evident when comparing the one-mode approximation $\Delta T_{c1}(=F_c)$ (Fig. 7(d)) with that in Fig. 7(c). Finally, shape of ΔT_{c1} in Fig. 7(d) matches that of u_c in Fig. 7(a) because for $\omega \ll \omega_{c1}$ the cable acts as a mass-less spring with stiffness $K_{c1} = E_c A_c / l_c$.

Fig. 8(a1–c1) plots beam and pendulum response excluding cable flexibility, and Fig. 8(a2–c2) plots incremental response from cable flexibility. In this example, a_b was increased by an order of magnitude to $a_b = 10$ cm from the case in Fig. 4 to magnify the effect of nonlinearity from pendulum swing. Comparing response in Fig. 8(a1 and b1) to that in Fig. 8(a2 and b2) reveals that Δw_L and ΔQ_{xxL} are 2 orders of magnitude smaller than linear response. Fig. 8(c1) shows that pendulum swing φl_c reaches $\varphi_{mx} \approx 0.25$ rad. Comparing Fig. 8(b1)–(c2) shows that magnitude of $Q_{xxL} = m_p l_c \ddot{\varphi}$ from pendulum inertia is 1/10 the incremental cable tension ΔT_c. However, the dominant frequencies in the ΔT_c response are much higher than the primary beam dyad $\omega_{cj} \gg \omega_1$, ω_2, $j \geqslant 1$. Although $|\Delta T_c| \gg |Q_{xxL}|$, the effect on flexural response of cable inertia is negligible. This result applies to a class of slender beams and pendulum mass sufficiently smaller than beam mass.

Fig. 9(b–d) plots response of coupled extensional motions of beam and cable for $\varphi_{mx} = 0.25$ rad from the centrifugal force in Fig. 9(a). Fig. 9(b and c) shows response of beam displacement $u_b(l_b)$ and axial force $T_b(l_b)$ during the first 5 s after start of motion. Note that T_b is more than an order of magnitude larger than F_c and this persists along the beam length as shown in Fig. 9(d) for $T_b(l_b/2)$. The dominant response frequencies are high compared to the driving frequency $2\omega_o$ although response is modulated by that frequency.

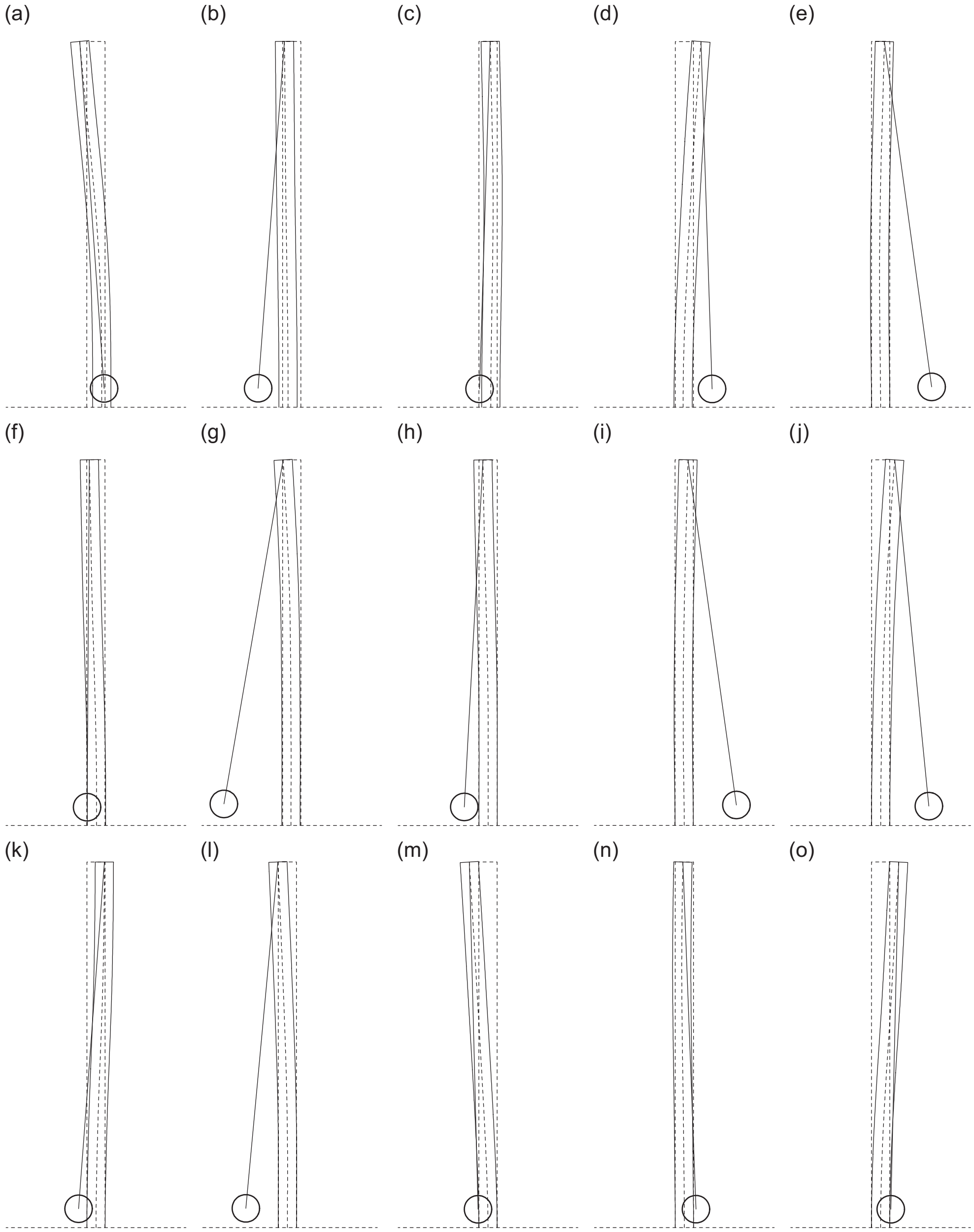

Fig. 6. Time snapshots of beam–pendulum. (a) $t = 0.5\,\text{s}$, (b) $t = 2\,\text{s}$, (c) $t = 3\,\text{s}$, (d) $t = 4\,\text{s}$, (e) $t = 5\,\text{s}$, (f) $t = 6\,\text{s}$, (g) $t = 7\,\text{s}$, (h) $t = 8\,\text{s}$, (i) $t = 9\,\text{s}$, (j) $t = 10\,\text{s}$, (k) $t = 11\,\text{s}$, (l) $t = 12\,\text{s}$, (m) $t = 13\,\text{s}$, (n) $t = 14\,\text{s}$ and (o) $t = 15\,\text{s}$.

5. Conclusion

The effect on response of a beam–pendulum system of cable flexibility is studied adopting modal analysis and the static–dynamic superposition method. Since the driving force to cable motions is nonlinear, a time-delayed method is adopted where cable tension is computed at time step t based on centrifugal force computed at a previous time step $t - \Delta t$. Noteworthy results of this study are:

1. Modal response relies on two non-dimensional parameters: a wave number $\kappa_o = l_b \left(m_b \omega_o^2 / (E_b I_b) \right)^{1/4}$ and a mass ratio $\mu_r = m_b l_b / m_p$.

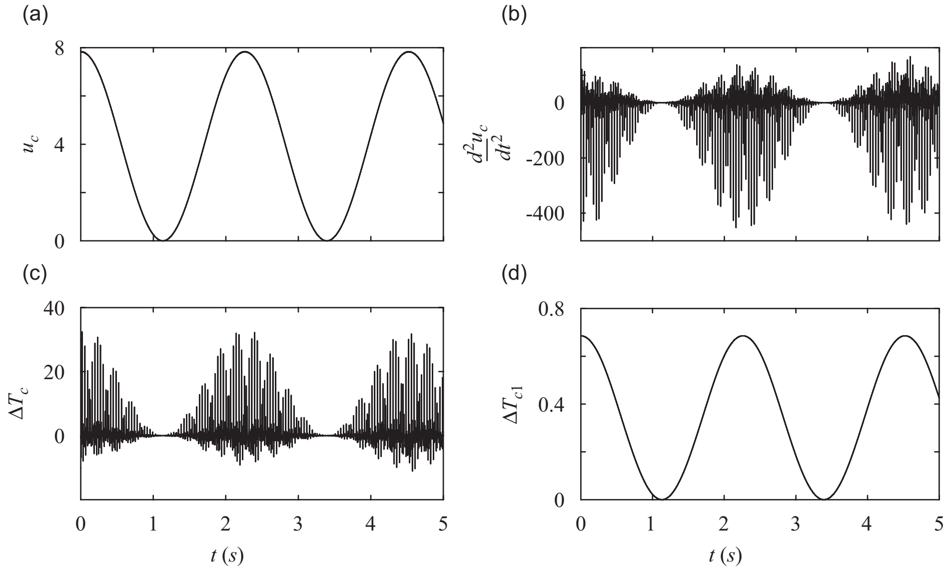

Fig. 7. Cable response from centrifugal force: $\phi_{mx} = 1$ rad. (a) $u_c(l_c)$ (cm), (b) $\mathrm{d}^2u_c/\mathrm{d}t^2$ (m/s^2), (c) ΔT_c (N) (25 terms), and (d) ΔT_{c1} (N) (1 term).

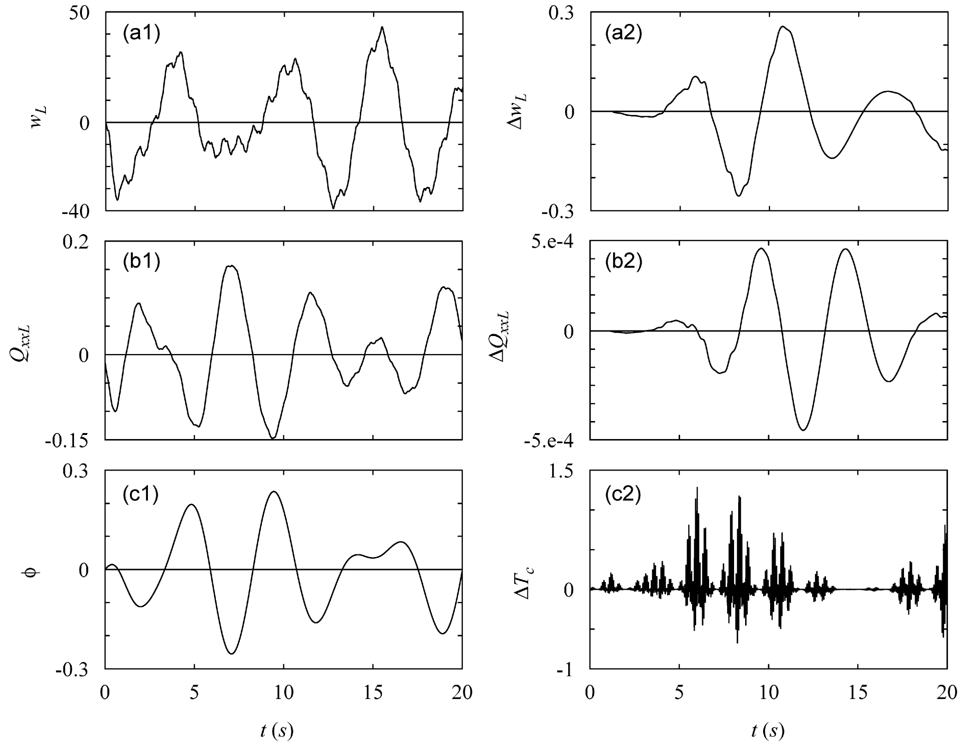

Fig. 8. Incremental response from cable inertia: $a_b = 10$ cm, $\phi_{mx} = 0.25$ rad. (a1) w_L (cm), (b1) Q_{xxL} (N), (c1) ϕ (rad.), (a2) Δw_L (cm), (b2) ΔQ_{xxL} (N), and (c2) ΔT_c (N).

2. The two primary modes or dyad influencing response are: a beam dominant mode $\omega_1 < \omega_o$ with beam and pendulum motions in phase, and a pendulum dominant mode $\omega_2 > \omega_o$ with beam and pendulum motions out-of-phase.

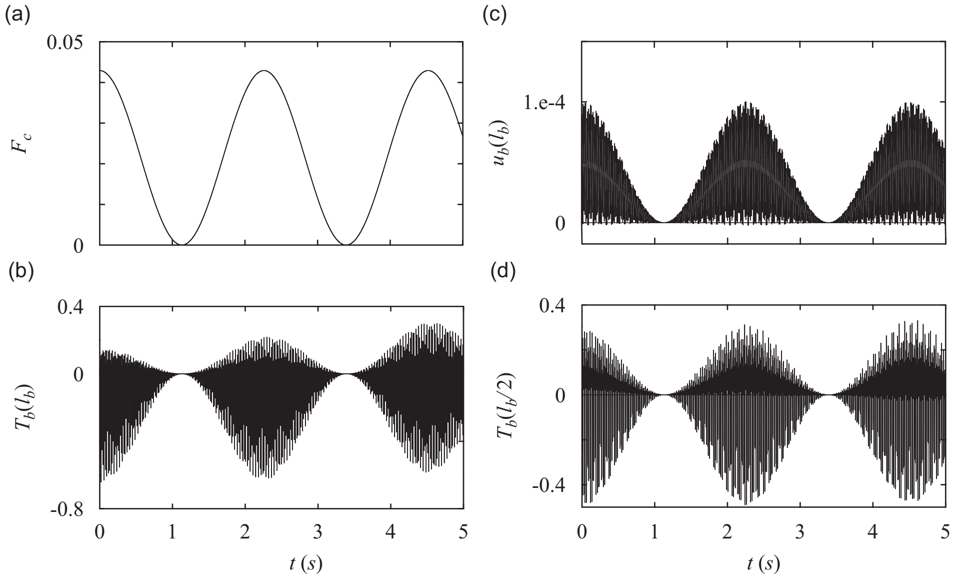

Fig. 9. Coupled beam–cable extensional motions: $\phi_{mx} = 0.25$ rad. (a) F_c, (b) $u_b(l_b)$, (c) $T_b(l_b)$, and (d) $T_b(l_b/2)$.

3. In curves of ω versus κ_o with μ_r as parameter, lines of different modes change path near coalition producing a change in nature of the mode. The value of κ_o near coalition is insensitive to μ_r. Coalition of the primary dyad occurs near $\kappa_o \approx 2$. Near this value, separation between the 2 frequencies in the dyad is smallest, affecting the transfer of energy between the 2 modes. The smaller μ_r is the wider this separation becomes.
4. Unlike vibration absorption achieved when periodic excitation coincides with the auto-parametric condition, in transient response energy transfer occurs within short time intervals when $\kappa_o \approx 2$.
5. Incremental cable tension ΔT_c from its flexibility and inertia may be much larger than reaction from pendulum inertia Q_{xxL}, yet its effect on flexural response is negligible because dominant frequencies in ΔT_c are much higher than those of the primary dyad.
6. In contrast to flexural response, cable tension has a noticeable effect on extensional motions of the beam, although response is still dominated by frequencies high compared to ω_o.

Appendix A. Pendulum equations with moving pivot

Lagrange's equations are

$$\frac{\mathrm{d}}{\mathrm{d}t}\frac{\partial L}{\partial \dot{q}_i} - \frac{\partial L}{\partial q_i} = 0, \quad L = T - P. \tag{A.1}$$

P, T are potential and kinetic energies and q_i are generalized coordinates. For the coupled system in Fig. 1(a)

$$T = \left(m_p\dot{r}^2 + m_p(r\dot{\varphi})^2\right)/2, \tag{A.2a}$$

$$P = m_p g l_c(1 - \cos(\theta)) = m_p g l_c\left(1 - \left(1 - (r\,\sin(\varphi) - w_L)^2/l_c^2\right)^{1/2}\right), \tag{A.2b}$$

where φ is the angle between undeformed beam axis B–A and cable r (B–C) from undeformed free end B to displaced pendulum mass C (Fig. 1(a)), and θ the angle between displaced cable B′–C and the vertical. The pivot moves from B to B′ by a displacement w_L. From Fig. 1(a)

$$r\,\sin(\varphi) = l_c\,\sin(\theta) + w_L, \tag{A.3a}$$

$$r = l_c\Big(1 + \big(\sin(\theta) + w_L/l_c\big)^2\Big)^{1/2}, \tag{A.3b}$$

$$\dot{r} = (l_c\ \sin(\theta) + w_L)\big(l_c\ \cos(\theta)\dot{\theta} + \dot{w}_L\big)/r, \tag{A.3c}$$

$$\begin{aligned}\ddot{r} = {} & \big(l_c\ \cos(\theta)\dot{\theta} + \dot{w}_L\big)^2\Big/r \\ & + (l_c\ \sin(\theta) + w_L)\Big(-l_c\ \sin(\theta)\dot{\theta}^2 + l_c\ \cos(\theta)\ddot{\theta} + \ddot{w}_L\Big)/r - \dot{r}^2/r.\end{aligned} \tag{A.3d}$$

P in Eq. (A.2b) is a function of θ only because when $\varphi = 0$, then from Eq. (A.3a) $\theta = \sin^{-1}(-w_L/l_c) \neq 0$ so although the mass is motionless along y yet it moves along x by $l_c(1 - \cos(\theta)) \approx l_c\theta^2/2$. Letting $q_1 = r$ and $q_2 = \varphi$ in Eq. (A.1) using Eq. (A.2) yields

$$m_p\ddot{r} - m_p r\dot{\varphi}^2 + m_p g\ \tan(\theta)\sin(\varphi) = F_r, \tag{A.4a}$$

$$m_p r^2\ddot{\varphi} + 2m_p r\dot{r}\dot{\varphi} + m_p gr\ \tan(\theta)\cos(\varphi) = rF_\theta. \tag{A.4b}$$

Linearizing Eq. (A.3) gives

$$\begin{aligned}&\varphi \approx \theta + w_L/l_c, \\ &r \approx l_c + o(l_c\theta^2), \quad \dot{r} \approx o(l_c\theta^2), \quad \ddot{r} \approx o(l_c\theta^2).\end{aligned} \tag{A.5}$$

This reduces Eq. (A.4) to

$$m_p l_c\big(\ddot{r}/l_c - \dot{\varphi}^2 + \omega_o^2\varphi(\varphi - w_L/l_c)\big) = F_r, \tag{A.6a}$$

$$m_p l_c\big(\ddot{\varphi} + \omega_o^2(\varphi - w_L/l_c)\big) = F_\theta. \tag{A.6b}$$

The reaction F_y along y at the pendulum pivot is

$$F_y = m_p l_c\ddot{\varphi}. \tag{A.7}$$

References

[1] M. Crespo da Silva, C. Zaretsky, D. Hodhges, Effects of approximations on the static and dynamic response of a cantelever with tip mass, *International Journal Solids Structures* 27 (5) (1991) 565–583.

[2] O. Cuvalci, The effect of detuning parameters on the absorption region for a coupled system: a numerical and experimental study, *Journal of Sound and Vibration* 229 (4) (2000) 837–857.

[3] A. Ertas, O. Cuvalci, S. Ekwaro-Osire, Performance of pendulum absorber for a non-linear system of varying orientation, *Journal of Sound and Vibration* 229 (4) (2000) 913–933.

[4] M. Yaman, S. Sen, O. Cuvalci, Finite element analysis of non-linear coupled oscillator, *Engineering Structures* 24 (5) (2002) 577–586.

[5] M. Yaman, S. Sen, The analysis of the orientation effect of non-linear flexible systems on performance of the pendulum absorber, *International Journal of Non-linear Mechanics* 39 (5) (2004) 741–752.

[6] M. Yaman, S. Sen, Determining the effect of detuning parameters on the absorption region for a coupled nonlinear system of varying orientation, *Journal of Sound and Vibration* 300 (1–2) (2007) 330–344.

[7] I. Cicek, A. Ertas, Experimental investigation of beam-tip mass and pendulum system under random excitation, *Mechanical Systems and Signal Processing* 18 (6) (2002) 1059–1072.

[8] J. Dumas, K. Lee, J. Winterflood, L. Ju, D. Blair, J. Jacob, Testing of a multi-stage low-frequency isolator using Euler spring and self-damped pendulum, *Classical Quantum Gravity* 21 (2004) 965–971.

[9] Y. Mikhlin, S. Reshetnikova, Dynamical interaction of an elastic system and essentially non-linear absorber, *Journal of Sound and Vibration* 283 (1–2) (2005) 91–120.

[10] D. Oguamanam, J. Hansen, G. Heppler, Dynamic response of an overhead crane system, *Journal of Sound and Vibration* 213 (5) (1998) 889–906.

[11] D. Oguamanam, J. Hansen, Dynamics of three-dimensional overhead crane system, *Journal of Sound and Vibration* 242 (3) (2001) 411–426.

[12] F. Ju, Y. Choo, F. Cui, Dynamic response of tower crane induced by the pendulum motion of the payload, *International Journal of Solids and Structures* 43 (2) (2006) 376–389.

[13] W. Yang, Z. Zhang, R. Shen, Modeling of system dynamics of a slewing flexible beam with moving payload pendulum, *Mechanics Research Communications* 34 (3) (2007) 260–266.
[14] R. Mindlin, L. Goodman, Beam vibrations with time dependent boundary conditions, *ASME Journal of Applied Mechanics* 17 (1950) 377–380.
[15] J. Berry, P. Naghdi, On the vibration of elastic bodies having time-dependent boundary conditions, *Quarterly of Applied Mathematics* 14 (1956) 43–50.